

# An Analysis of Sea Level Spatial Variability by Topological Indicators and $k$ -means Clustering Algorithm

Zixin Lin, Nur Fariha Syaquina Zulkepli\*, Mohd Shareduwan Mohd Kasihmuddin, R. U. Gobithaasan

**Address:** School of Mathematical Sciences, Universiti Sains Malaysia, 11800 USM, Penang, Malaysia

**Email:** \*farihasyaqina@usm.my

## Abstract

The time-series data of sea level rise and fall contains crucial information on the variability of sea level patterns. Traditional  $k$ -means clustering is commonly used for categorizing regional variability of sea level, however, its results are not robust against a number of factors. This study analyzed fourteen datasets of monthly sea level in fourteen shoreline regions of Peninsular Malaysia. We applied a hybridization of clustering technique to analyze data categorization and topological data analysis method to enhance the performance of our clustering analysis. Specifically, our approach utilized the persistent homology and  $k$ -means/ $k$ -means++ clustering. The fourteen data sets from fourteen tide gauge stations were categorized in classes based on a prior categorization that was determined by topological information, and the probability of data points that belong to certain groups that is yielded by  $k$ -means/ $k$ -means++ clustering. Our results demonstrated that our method significantly improves the performance of traditional clustering techniques.

**Keywords:** Machine learning, Computational topology, Environmental sustainability, Sea level variability

## 1 Introduction

As a result of global warming and human activities, such as land reclamation, the global mean sea level has been rising significantly [1]. Malaysia, with over two thousand kilometers of coastal regions, is not exempt from this trend. The impact of global warming and human activities on rising sea levels has profound implications for Malaysia's coastal areas. However, the rise is non-uniform due to various primary factors, such as geographical differences. This non-uniformity

complicates the prediction of sea level changes in specific regions, the implementation of marine management policies, and ecosystem protection efforts [2].

This study focuses on Peninsular Malaysia, which is situated in the heart of Southeast Asia. Bounded by the Malacca Strait to the west, the South China Sea to the east, and the Singapore Strait to the south, Peninsular Malaysia's unique geographical location adds to the regional variations in sea level variability (see more details in [3], [4]). The change in sea level is influenced by various regional phenomena in the adjacent parts of the Indian and Pacific Oceans, as well as by wind and weather patterns in the South China Sea and the Indian and Pacific Oceans [5]. These regional factors and weather patterns complicate the estimation of temporal and spatial variability in sea level change in Peninsular Malaysia. An important step in estimating and predicting sea level rise is by identifying the patterns of sea level variability in different regions. This is crucial for many reasons, like understanding the impact of rising sea levels on coastal communities, ecosystems, and infrastructure. Such information is essential for effective coastal planning and adaptation strategies [4].

There are numerous works that have been exploring and studying sea level data sets. Kumar et al.,(2010) [6] explored the reconstruction of sea levels in locations of the western south Pacific by multiple linear regression of atmospheric and oceanic variables. Imani et al.,(2014) [7] studied Caspian sea level forecasting at various time intervals by supporting vector machine and gene expression programming. Song et al.,(2021) [8] performed sea level simulations with mode decomposition and the Elman neural network. den Bieman et al.,(2023) [9] proposed an innovative hybrid modelling approach to improve the accuracy of operational wave forecasts. Jiang et al.,(2024) [10] tested the dynamic response of intermediate-scale physical semi-submersible FOWT model. While many studies have analyzed sea level variability using traditional learning techniques (see [11], [12] for more examples), most of them relied on pre-assumed models and variables or did not consider the shapes of the data analyzed.

The motivation for combining  $k$ -means or  $k$ -means++ clustering with persistent homology in data analysis stems from the widespread use of  $k$ -means clustering as an unsupervised machine learning algorithm for partitioning datasets into clusters [13]. While  $k$ -means is known for its simplicity of implementation and scalability, it is not without its drawbacks. Specifically,  $k$ -means is sensitive to the initial selection of centroids, and its performance can degrade when applied to certain types of data (see more details in section 2.3). By integrating persistent homology with  $k$ -means clustering, it becomes possible to leverage the strengths of both methods: the efficiency and scalability of  $k$ -means and the ability of persistent homology to capture topological features across different scales in the data. This combined approach aims to enhance the clustering process

by providing a more robust and comprehensive analysis of complex datasets [14] (see more details in section 2.5).

This study aims to analyze the patterns of sea level variability in sea regions of Peninsular Malaysia using a hybrid approach that combines  $k$ -means/ $k$ -means++ clustering and persistent homology from topology data analysis (TDA). Another motivation is advantages of persistent homology. Persistent homology is a powerful tool in topological data analysis that's used to extract qualitative features, or topological features, from data sets. What makes persistent homology particularly useful is its ability to capture features that persist across multiple scales. This means it can identify important topological structures in data that might not be immediately apparent from a single-scale analysis [15]. In other words, persistent homology and many other topological analyzing methods may help researchers better to decipher the complicated structure of data (see more details in [16]). By analyzing the evolution of these features across different scales, persistent homology provides a richer understanding of the underlying topology of the data. See [17], [18], [19], [20], [21] for more applications of TDA.

To the best of our knowledge, there has been no exploration of cluster analysis incorporating topological information, particularly the combination of  $k$ -means clustering with persistent homology, in studies of sea level rise. Therefore, this study aims to assess the effectiveness of clustering techniques with and without topological information in analyzing patterns of sea level variability (see more details in sections 3.1 and 3.2). This is also a significant consideration in many studies related to heavy rainfall. Heavy rainfall can indirectly contribute to sea level rise by increasing runoff into oceans and accelerating the melting of glaciers, which then adds freshwater to the ocean. While not a direct cause, heavy rainfall can exacerbate the impacts of sea level rise by influencing ice sheet dynamics and increasing freshwater input into coastal areas. (see more details in [22], [23], and [24]).

In our study, we applied the hybrid approach described in Algorithm 1 to analyze fourteen distinct time-series datasets representing sea level measurements from fourteen different tide gauge stations. To illustrate the flow of our methodology, we presented results for six shoreline regions in section 3.2, deliberately choosing two datasets from each of the east coast, west coast, and southern region of Peninsular Malaysia. It's important to note that the selection of these specific six datasets from the fourteen tide gauge stations was arbitrary. Subsequently, in section 3.3, we expanded our analysis to include results for all fourteen sea regions.

Our analysis methodology is not limited to these datasets and can be applied to any time-series data representing sea level changes. Besides, the method used in this study enables us to pinpoint coastal areas that exhibit comparable patterns in mean sea-level fluctuations. Consequently, we

can employ this approach to investigate variations in how different regions respond to the overall rise in global sea levels resulting from either global warming or extensive polar ice melting [25]. Our expectation was that the datasets from different coastal regions would be classified into distinct clusters using our hybrid approach. This hypothesis was based on the assumption that sea level changes in different coastal areas exhibit unique patterns, which our method aims to capture. Our approach also contributes to the estimation and prediction of sea level changes. For instance, in regions with sufficient historical data, reliable predictions of future sea levels can be made [26]. Then, if other regions demonstrate similar patterns of sea level rise and fall, these predictions can be applied to areas with less reliable historical data to support their predictions. Moreover, our approach suggests that the precise positioning of tide gauges (often along the coast or in harbors) significantly influences observed sea level fluctuations. This finding holds particular relevance for studies employing machine learning techniques to analyze sea level patterns. For instance, certain machine learning methods assign varying weights to different variables, such as temperature or location, in their models [27]. Our approach underscores the importance of giving location a significant weight due to its dominant role in shaping sea level patterns.

The paper is structured as follows: In Section 2, we present the selection of datasets and discuss the backgrounds of  $k$ -means/ $k$ -means++ clustering and persistent homology. Section 3 presents the results of our study, compares the effectiveness of the traditional clustering method with our hybrid approach, and demonstrates how the results align with our initial hypothesis. In Section 4, we interpret our results through the lens of ocean science. Finally, we summarize the work in this paper in Section 5.

## 2 Data and Methodology

### 2.1 Data

The land of Peninsular Malaysia is surrounded by approximately 2,068 kilometers (1,285 miles) of coastline, offering a diverse range of landscapes and ecosystems. The shores of Peninsular Malaysia are divided into three major regions - west coast, east coast, and southern region, respectively, which experience various monsoon seasons. In fact, Malaysia monsoon seasons can be divided into two prominent periods. One is the Nov-March Northeast Monsoon that dominates in east coast, and other May-Sept Southwest Monsoon that dominates in west coast (see more details in <https://www.met.gov.my/en/pendidikan/iklim-malaysia/>).

The data applied in this study consists of fourteen data sets that come from fourteen different tide gauge stations in different shoreline regions. The Table 1 shows names of tide gauge locations,

Table 1: The names, coastal locations, latitude, and longitude of fourteen different tide gauge stations; the red colored entries indicate chosen regions for illustrating the flow of methodology.

Location	Latitude	Longitude	Coastal Region
Geting	6.22	102.11	East
Cendering	5.26	103.19	East
Gelang	3.97	103.43	East
Tioman	2.81	104.14	East
Sedili	1.93	104.11	East
Langkawi	6.43	99.76	West
Pinang	5.42	100.35	West
Lumut	4.24	100.61	West
Kelang	3.05	101.36	West
Keling	2.21	102.15	West
Kukup	1.33	103.44	West
Shoal	1.23	103.65	Southern
Sembawang	1.47	103.83	Southern
Pagar	1.27	103.85	Southern

their coastal locations, latitudes, and longitudes, while Figure 1 and Figure 2 shows their specific locations in two maps. The tide gauges stations are evenly chosen along the peninsular coast in three sea regions - five tide gauge stations (Geting, Gelang, Cendering, Tioman, and Sedili) from east coast, six tide gauge stations (Langkawi, Pinang, Lumut, Kelang, Keling, and Kukup) from west coast, and three tide gauge stations (Sembawang, Pagar, and Shoal) from southern region. It's worth noting that there are some differences between the names shown on the maps and the names we have used in our paper. Specifically, for the simplicity and consistency with the names used on the website from which our data originates, we refer to Tg.Keling as Keling, Port Kelang as Kelang (names in each pair (e.g. Port Kelang and Kelang) refer to the same place, and could be used interchangeably), and we did not include Bahru in our study; instead, we used Sembawang. Without ambiguity, in the remainder of this paper, we used the names of tide gauge stations as references to the sea regions where they are located. In Figure 2, we present more precise locations of Sembawang, Pagar and Shoal in an enlarged map of Singapore. It is evident that the sea region indicated by Sembawang is situated between two land masses and is quite narrow, resembling a river. In Table 1, we have highlighted the six sea regions in red to signify them as the selected ones for the analysis presented in section 3.2. These regions were chosen as illustrative examples to demonstrate the flow of our methodology.

Each data set contains monthly mean sea level (MMSL) records from its corresponding tide gauge station in a period from January, 1989 to December, 2018. This means that a total of 5040 (30 years  $\times$  12 months  $\times$  14 stations) historic data related to the monthly mean sea level events are collected and applied in this study. The Figure 3 show boxplots of the selected sea regions.

The data sets applied in this research all were obtained from the Permanent Service for Mean Sea Level (PSMSL; <http://www.psmsl.org/data/obtaining/> [28]).

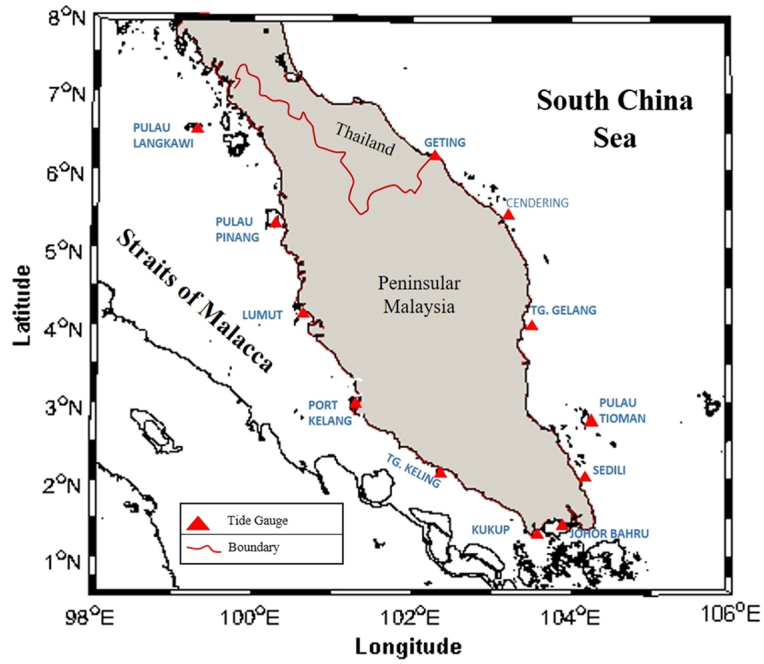


Figure 1: The map [29] of locations of the studied stations in West Malaysia.



Figure 2: The zoomed-in map of the studied locations (Sembawang, Pagar, and Shoal indicated by red arrows).

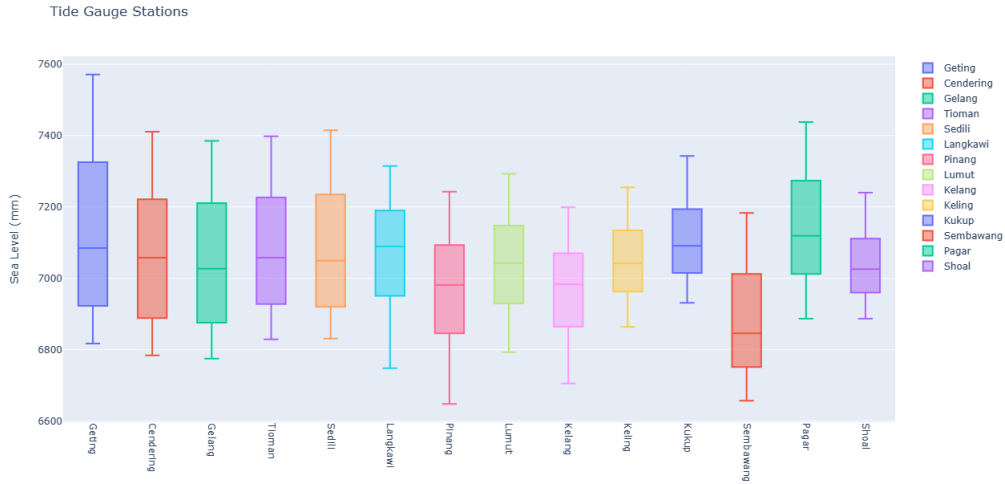


Figure 3: Boxplots of the studied locations between January, 1989 to December, 2018.

## 2.2 Taken's Embedding Theorem

Undoubtedly, the sea level variability over a period in a given region is nonlinear with respect to time and appears as a time-series pattern. To study the patterns of sea level variability as using clustering and homology features, we require transition rules and attractors to convert the time-series data, into a point cloud data. One method to achieve this is by using forecast density and h-step-ahead predicted values [30] to build a dissimilarity matrix that represents distances. However, this method requires assuming and defining a model for each time series under analysis, which can complicate the task. Another method commonly used in conjunction with the  $k$ -Nearest Neighbor method is dynamic time warping (DTW). However, DTW is known to be sensitive to noise and is generally unsuitable for analyzing chaotic time-series data [31], such as that often encountered in sea level variability studies.

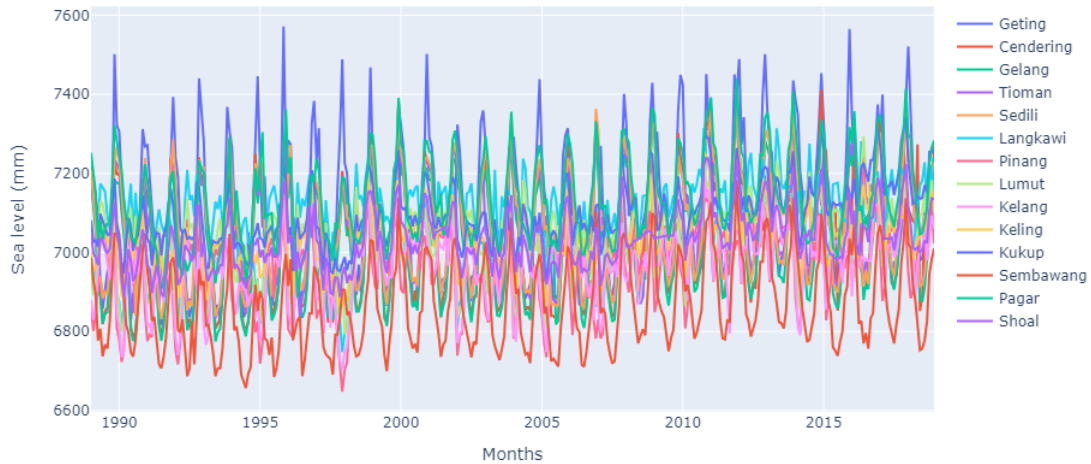


Figure 4: Time series from data obtained in fourteen tide gauge station, and one example of them is embedded as a point cloud in phase space, which is shown in the Figure 5.

As we delve deeper into the qualitative analysis of the series without depending on any predetermined models, we employ Takens' embedding theorem (the Quasi-attractor) to reconstruct time-series data in phase space [32]. This technique is applicable for time-series data represented as continuous curves or surfaces, transforming them into point cloud data in phase space. By carefully selecting suitable parameters such as  $m$  (embedding dimension) and  $\tau$  (time delay), a series  $x_0, x_1, \dots, x_{n-1}$  can be transformed into its phase space representation  $X_n(m, \tau) = (x_n, x_{n+\tau}, \dots, x_{n+(m-1)\tau})$  [18]. For example, we applied this method to a time series using data from Sembawang, resulting in the creation of a point cloud in phase space. Additional details are provided in Figure 4 and 5. Consequently, rather than analyzing the series over time, we examine its trajectory as a set of visited states in an  $m$ -dimensional Euclidean space. This approach offers significant advantages for analyzing data through clustering and extracting relevant topological behaviors.

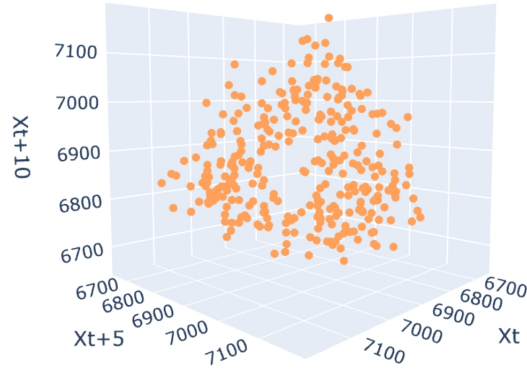
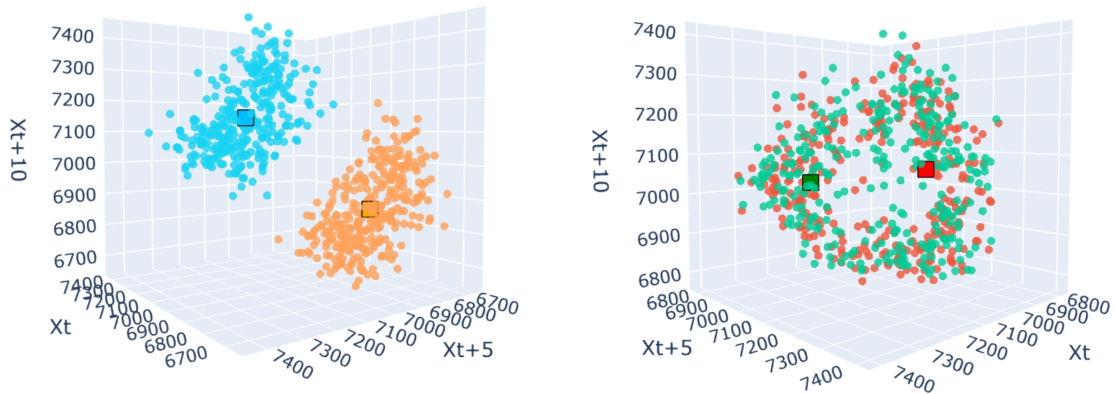


Figure 5: A 3-dimensional point cloud data ( $\tau = 5, m = 3$ ) embedded from one of time series shown in Figure 4 for Sembawang station.

### 2.3 $k$ -means/ $k$ -means++ Clustering

The  $k$ -means clustering is a popular unsupervised machine learning algorithm used for clustering similar data points into groups or clusters. The algorithm works by partitioning the data into  $k$  clusters, where each data point belongs to the cluster with the nearest mean.  $k$ -means clustering aims to minimize the within-cluster sum of squares (WCSS), which is the sum of the squared distances between each data point and its assigned centroid [33]. The algorithm seeks to find centroids that minimize this value, effectively grouping similar data points together. It's important to note that  $k$ -means clustering is sensitive to the initial choice of centroids and can converge to a local minimum [34], so it's common to run the algorithm of its variant,  $k$ -means++, with different initialization and choose the best result based on some criteria (e.g., minimum WCSS).



(a) Two sets of data from Sembawang and Pagar, colored by light blue and orange respectively, can be well categorized by  $k$ -means/ $k$ -means++ clustering, and the squares indicate the centroids generated by  $k$ -means clustering.

(b) Two sets of data from Gelang and Cendering, colored by green and red respectively, cannot be categorized by  $k$ -means/ $k$ -means++ clustering, and the squares indicate the centroids generated by  $k$ -means clustering.

Figure 6: An illustration of the scenario where the performance of  $k$ -means/ $k$ -means++ clustering diminishes extremely when data sets are well mixed.

While  $k$ -means clustering, including its variant  $k$ -means++, performs well when categorizing data sets with distinct centroids and minimal noise, its performance diminishes when applied to datasets where groups are mixed or have significant noise. For example, consider a set of point cloud data  $(u_{ij})_{1 \leq i \leq n, 1 \leq j \leq m}$ , each sample  $\mathbf{u}_i = (u_{ij})_{1 \leq j \leq m}$  is generated by  $\mathbf{u}_i = \mathbf{u} + \alpha_i$  with  $\mathbf{u}$  representing the distribution mean and  $\alpha_i$  representing noise. Even if  $\{\alpha_i\}_{1 \leq i \leq n}$  could share the same distribution in some cases, if they exhibit a large variance,  $k$ -means clustering may output multiple different centroids and categorize the data into more than one group. Another scenario where the performance of  $k$ -means/ $k$ -means++ clustering diminishes extremely is when data clouds are well mixed and is illustrated in Figure 6. For data points that are less separable, we can use a kernel function to map them into a higher-dimensional space where they become separable. However, when dealing with data points like those shown in Figure 6b, where two clouds are highly mixed, this approach is not suitable.

In our work, we used persistence homology introduced in the next subsection to improve the performance of  $k$ -means/ $k$ -means++ clustering.

## 2.4 Persistent Homology

Persistent homology was applied to the point cloud data  $P = \{v_1, \dots, v_n\}$ . We assumed the point cloud data  $P$  is produced by applying Takens's theorem on time series data of sea level variability and it is a subset of a metric space  $(Z, d_Z)$ <sup>1</sup>. A  $p$ -dimension simplex or  $p$ -simplex of  $p + 1$  points  $\{v_{k_1}, \dots, v_{k_p}\} \subseteq P$  denoted by  $\sigma_p$  is the minimum convex hull containing the points. In the context of topology, we call the points in  $P$  vertices. Therefore, an 0-dimension simplex is a vertex itself, a 1-dimension simplex is an edge connecting two vertices, a 2-dimension simplex is a triangle, and a 3-dimension simplex is a tetrahedron. A simplicial complex is a set of simplices following Definition 1 [17]. Figure 7 shows a geometric realization of a simplicial complex embedded in 2-dimension Euclidean space.

**Definition 1.** *A simplicial complex  $K$  is a set containing finitely many simplices that satisfies the following two restrictions.*

- For a simplex  $\sigma \in K$ , any subsimplex  $\tau \subseteq \sigma$ , which are called the face of  $\sigma$ , are also contained in  $K$ .
- For any two simplices  $\sigma_q, \sigma_p$  contained in  $K$ , their intersection  $\sigma_q \cap \sigma_p$  is either an empty set or a face of both  $\sigma_q$  and  $\sigma_p$ .

---

<sup>1</sup>In this paper, we take  $Z$  as Euclidean space  $\mathbb{R}^n$ . The metric  $d_Z$  measures the norm of any vector or distance between any pair of vectors  $x, y \in Z$ , in Euclidean space,  $d_Z$  is usually taken as  $L^r$  so that  $\|x\|_r = (\sum x_i^r)^{1/r}$  for any vector  $x = (x_1, \dots, x_n) \in Z$ . In this paper, we take metric  $d_Z$  as  $L^2$ .

The dimension of  $K$  is defined as the maximum dimension of its simplices.

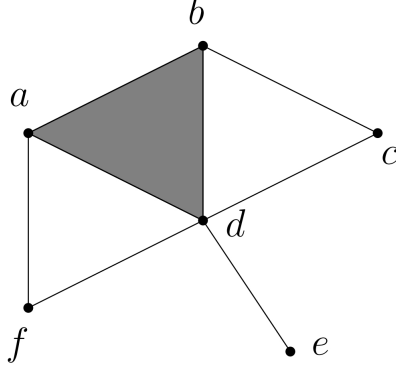


Figure 7: A simplicial complex with six vertices  $\{a\}, \{b\}, \{c\}, \{d\}, \{e\}, \{f\}$  as 0-dimension simplices, eight edges  $\{a, b\}, \{a, d\}, \{a, f\}, \{b, c\}, \{b, d\}, \{c, d\}, \{d, e\}, \{d, f\}$  as 1-dimension simplices, and one triangle  $\{a, b, c\}$  as 2-dimension simplex [17].

A filtration  $\mathcal{F} = \mathcal{F}(K)$  of a simplicial complex  $K$  is a nested sequence written with inclusion maps (continuous functions) as  $\mathcal{F} : \emptyset = K_0 \hookrightarrow K_1 \hookrightarrow \dots \hookrightarrow K_n = K$ . One of the commonly used complexes is Vietoris-Rips complex [35]. For a given data point cloud  $P$ , Vietoris-Rips complex is defined as  $\text{VR}_\epsilon(P) = \{\sigma \subseteq P \mid \text{diam}(\sigma) < 2\epsilon\}$ . The definition indicates that the Vietoris-Rips complex of point cloud  $P$  is the collection of all subsets of point whose diameter measured by  $d_Z$  is not greater than  $2\epsilon$ . One can construct a filtration of Vietoris-Rips complexes by increasing  $\epsilon$ , see more details in Figure 8. And  $P$  is usually omitted in  $\text{VR}_\epsilon(P)$ , when the context is clear. For the coefficients field from  $R$ -module  $\mathbb{Z}_R$ , a  $p$ -chain is defined as  $C_p = \{c_p \mid c_p = \sum_{i=1}^{m_p} \alpha_i \sigma_p^i, \alpha_i \in \mathbb{Z}_R\}$ , where  $m_p$  represents the number of  $p$ -simplices contained in  $K$ . When  $p < 0$  or  $p > n$ ,  $C_p = \emptyset$ . Given a  $p$ -simplex  $\sigma_p = \{v_0, \dots, v_p\}$ , the boundary operator  $\partial_p : C_p \rightarrow C_{p-1}$  is defined as  $\partial_p c_p = \sum_{i=1}^{m_p} \alpha_i (\partial_p \sigma_p^i)$  for a  $p$ -chain  $c_p = \sum_{i=1}^{m_p} \alpha_i \sigma_p^i \in C_p$ , where  $\partial_p \sigma_p = \sum_{i=0}^p \{v_0, \dots, \hat{v}_i, \dots, v_p\}$  and  $\hat{v}_i$  indicates that it is removed. Then the cycle group is defined as:  $Z_p = \{c_p \in C_p \mid \partial_p c_p = 0\}$ , and boundary group as:  $B_p = \{c_p \in C_p \mid \exists c_{p+1} \in C_{p+1} \text{ so that } \partial_{p+1} c_{p+1} = c_p\}$ , and homology group given by  $H_p = Z_p / B_p$  and its dimension is called the  $p$ -th Betti number [17].

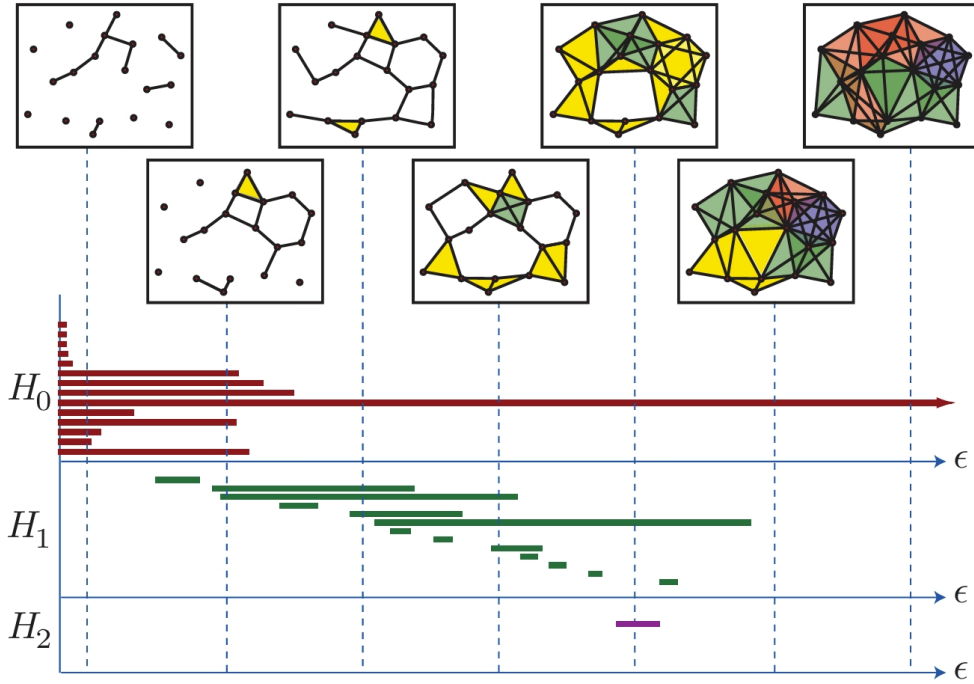


Figure 8: An example of Vietoris-Rips complex filtration with growing  $\epsilon$ , and barcodes indicate birth-death pairs  $d_i - b_i$ . The seven figures from left to right above the barcode plot indicates a filtration of Vietoris-Rips complex as  $\epsilon$  increases. The rank (the Betti number) of  $H_k(\text{VR}_{\epsilon_0})$  equals the number of intervals in the barcode for  $H_k(\text{VR})$  intersecting the dashed line  $\epsilon = \epsilon_0$  [35].

Corresponding to a filtration of complex, a sequence of homology groups is called homology module and defined as:  $0 = H_p(K_0) \rightarrow \cdots \rightarrow H_p(K_i) \xrightarrow{h_p^{i,j}} H_p(K_j) \cdots \rightarrow H_p(K)$ , where  $h_p^{i,j}$  denotes the inclusion map sending cycles in  $H_p(K_i)$  to  $H_p(K_j)$  for any  $0 \leq i \leq j \leq n$ .

It is well-known that as the index  $i$  increases, persistent homology groups capture the information about the shapes of the original data space  $X \subseteq Z$  from which our point cloud data originates. More specifically, a persistent homology module and its persistence diagram reveal the birth  $b_i$  and death  $d_i$  of homology classes that exist in the vector space  $p$ -chain and are not boundaries (see more details in Figure 8). This implies that we can utilize the information about the shape of each group of point cloud data to enhance the performance of  $k$ -means/ $k$ -means++ clustering for groups that are poorly categorized by  $k$ -means clustering or its variants.

## 2.5 Hybridization of $k$ -means/ $k$ -means++ Clustering and Persistent Homology

The  $k$ -means clustering categorizes data by computing distances and centroids between different data sets. However, it requires complementary information to correctly categorize data groups with large variances or those that are mixed together. On the other hand, persistence homology qualifies

the shapes' information, which can be represented as feature vector at point cloud. Therefore, these two methods complement each other. The philosophy behind using a hybridization of  $k$ -means clustering and persistence homology to analyze time-series data is that point cloud data with distinct topological shapes should exhibit distinct patterns of sea level variability. However, point clouds with the same or similar topological shapes do not necessarily belong to the same categories. In addition to shapes, it is essential to consider the dissimilar measure and centroids between classes of data generated by  $k$ -means clustering.

The first step is to generate groups of point cloud data using the Takens' Embedding Theorem. The second step involves building a complex and filtration. Several candidates for complexes exist, such as Cubical Complexes, Alpha Complexes, Witness Complexes, Vietoris–Rips or Čech Complexes. In this work, we use the Vietoris–Rips (VR) complex as the default. Once the complexes and filtration are computed, summarized in the persistence diagram, we compute a set of geometrical and topological features to characterize the time series.

We define the persistence diagram as a multiset  $\Pi \in \{\pi_0, \pi_1, \dots, \pi_n\}$ , where each  $\pi_i = (b_i, d_i)$  represents the birth value  $b_i$  and death value  $d_i$  of a feature  $i$ . Since we are mainly concerned with the shapes of the data point cloud, we focus on 1-dimensional holes ( $H_1$  features). We then extract features from each persistence diagram. When determining the shape of a point cloud, there are various criteria that can be considered. For instance, the Betti sequence is often utilized in non-chaotic time-series classification. However, it's important to note that the betti sequence can be sensitive to chaotic noises, as discussed in more detail in [37]. The other feature is the maximum hole lifetime in each dimension, representing the longest-lasting feature in the filtration. Short lifetimes are referred to as “geometric features”, while long lifetimes are recognized as “topological features” [38]. Therefore, we use the maximum hole lifetime to determine the topological shape of data sets, and it is defined as

$$\max_d = \max_{\pi_i \in \Pi} (d_i - b_i). \quad (1)$$

After obtaining the shape information of the point cloud data, we further consider classes that share the same or similar topological shapes and apply the  $k$ -means algorithm to them. For each class of point cloud data  $G_i$ , we define  $N_j$  as the number of points in  $G_i$  that belong to the  $j$ -th cluster  $C_j$ , and we define

$$P_i = \max_j \frac{N_j}{\sum N_i}, \quad (2)$$

where  $N_j$  represents the number of points in data group that belong to a certain cluster, and  $\sum N_i$  denotes the total number of points in data class in  $G_i$ . Therefore,  $P_i$  indicates the largest

percentage of points in data group  $G_i$  that belong to a certain cluster. Technically speaking, based on a loss function minimized by maximum likelihood estimate, if  $P_i$  is sufficiently large, it implies that data class  $G_i$  can be reliably categorized into the cluster with  $P_i$ . Additionally, for each category  $C_j$ , we define its centroid as  $c_j$ . The pseudo-codes for the Hybridization of  $k$ -means Clustering and Persistence Homology (HKCPH) are provided in Algorithm 1, and our working pipeline is illustrated in Figure 9.

It is important to clarify that we do not assign any specific physical meaning to individual cluster. These clusters do not represent specific magnitudes of sea level rise or fall. Instead, the categorization of data sets into different clusters signifies that they exhibit distinct patterns of variability in sea level. Each cluster captures a unique behavior or trend in the sea level data, allowing us to discern different patterns of variability across the data set.

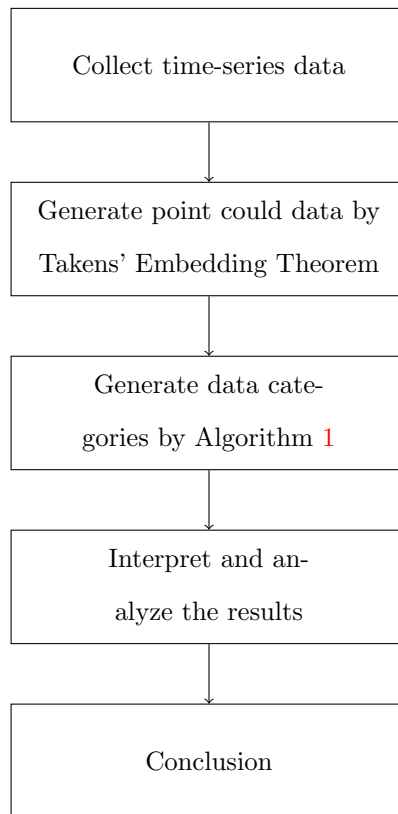


Figure 9: Working Pipeline.

---

**Algorithm 1: HKCPH**

---

**Input:** Point cloud data generated by Embedding Theorem, the type of complex used (default Vietoris-Rips (VR) complex defined over 3-module  $\mathbb{Z}_3$ ), dissimilar measure  $d_Z$  (default as  $L^2$ ), shape-determining criterion (default maximum lifetime), and two constants  $C$  and  $P$  (Eq.1, default 0.65).

**Result:** A dictionary with categories and data groups.

initialization;

**for** each class of point cloud data **do**

    build selected complex and compute and extract persistence diagram from  $H_1$ ;  
    determines its shape by its max lifetime for Eq.1;

**end**

**for** data sets sharing the same or similar shape **do**

    run  $k$ -means/ $k$ -means++ algorithm for them;  
    **if** ( $d_Z(c_i, c_j) > C$  for centroids  $c_i, c_j$ ) and ( $P_i > P$  and  $P_j > P$ ) **then**  
        assign  $C_i, C_j$  into different categories;  
    **else**  
        assign them into the same category;  
    **end**

**end**

**for** data sets with distinct shape vectors **do**

    assign them into different categories;

**end**

**return** a dictionary with keys as categories and values as names of tide gauge station.

---

1     The time and space complexity of Algorithm 1 depends on subordinate algorithms used for  
2     computing  $k$ -means clustering and Vietoris-Rips complexes, data structures used for storing clus-  
3     ters and vectors, type of machine on which we run the algorithm. For example, the running time of  
4     standard  $k$ -means algorithm is  $O(knm)$ , where  $m$  is the number of data points,  $n$  is the dimension  
5     of each point, and  $k$  is the pre-determined number of clusters. If one uses lower-star simple-  
6     wise filtration and Mat-Persistence algorithm [17] to build Vietoris-Rips complexes and compute  
7     persistence diagrams, the running time is  $O(N^3)$ , where  $N$  is the number of simplices in the bound-  
8     ary matrix. In this paper, we used packages SciPy and `scipy.kmeans/kmeans2`(<https://scipy.org/>  
9     [39]) to compute  $k$ -means clustering, `giotto-tda` and `gtda.homology.VietorisRipsPersistence`  
10    (<https://giotto-ai.github.io/gtda-docs/0.5.1/index.html> [40]) to compute persistence module of  
11    Vietoris-Rips complexes, and hash-based dictionary to store shapes, clusters and embedded data

12 sets so that many basic operations can be completed in expected constant time.

### 13 **3 Results**

14 Initially, we utilized six specific data sets represented by the red-colored station names in Table 1 to  
15 demonstrate the flow of our methodology, as outlined in Algorithm 1. This demonstration aimed to  
16 showcase how our hybrid approach enhances the performance of traditional  $k$ -means/ $k$ -means++  
17 clustering. Subsequently, we expanded our analysis to include all fourteen stations and presented  
18 the results in section 3.3. The optimal dimensions and time delays for time-series data can vary  
19 significantly depending on the data’s nature. However, it is not suitable to transform time-series  
20 data sets with different attractors [41]. Therefore, in this paper, we assigned fixed values to the  
21 dimension and time delay. We fixed the dimension  $m = 3$  and  $\tau = 5$  for the six data sets. As  
22 an attempt to show robustness of our method, we fixed  $\tau = 8$  when applying the hybridization  
23 method to fourteen data sets. The selection of  $\tau = 5$  and  $\tau = 8$  has two reasons. First, the weather  
24 in Malaysia is characterized by two monsoon regimes, namely the Southwest Monsoon that starts  
25 from late May to September, and the Northeast Monsoon from November to March [42], which  
26 lasts around 5 months, so that selections of  $\tau = 5$  or  $\tau = 8$  cover the periods of monsoons that play  
27 key roles in Malaysia’s climate and sea level changes. Second, selecting  $\tau = 8$  in fourteen stations  
28 case is an attempt to demonstrate the robustness of our method.

29 Subsequently, we transformed six time-series datasets obtained from PSMSL, covering the  
30 period from January 1989 to December 2018, into point cloud data. These data sets are visualized  
31 in Figure 10 and its subfigures. In the visualization, each set is represented by a different color.  
32 It is important to note that we refer to tide gauge stations by name as a reference to the sea  
33 regions where the data were collected. Figure 10g combines these six groups of data into a single  
34 three-dimensional Cartesian coordinate system diagram. In the subsequent subsections, we initially  
35 employed traditional  $k$ -means or  $k$ -means++ clustering to categorize the six sets of point cloud  
36 data. Our findings revealed that, regardless of the choice of the parameter  $k$  for  $k$ -means clustering,  
37 certain groups could not be effectively classified. In other words, we could not identify a  $P_i$   
38 (as described in Eq.2) for some data sets that was consistently larger than others, making it  
39 unreasonable to assign these data sets to specific classes.

40 In the second subsection, we improved the overall performance by utilizing Algorithm HKCPH  
41 (Al.1). This method involved encoding and analyzing the shape of point cloud data. The results  
42 demonstrated that by employing this approach, we could achieve well-defined and well-supported  
43 categorizations of sea level changes that were both explainable and resilient against perturbations

44 from noise (further details are provided in the subsequent section).

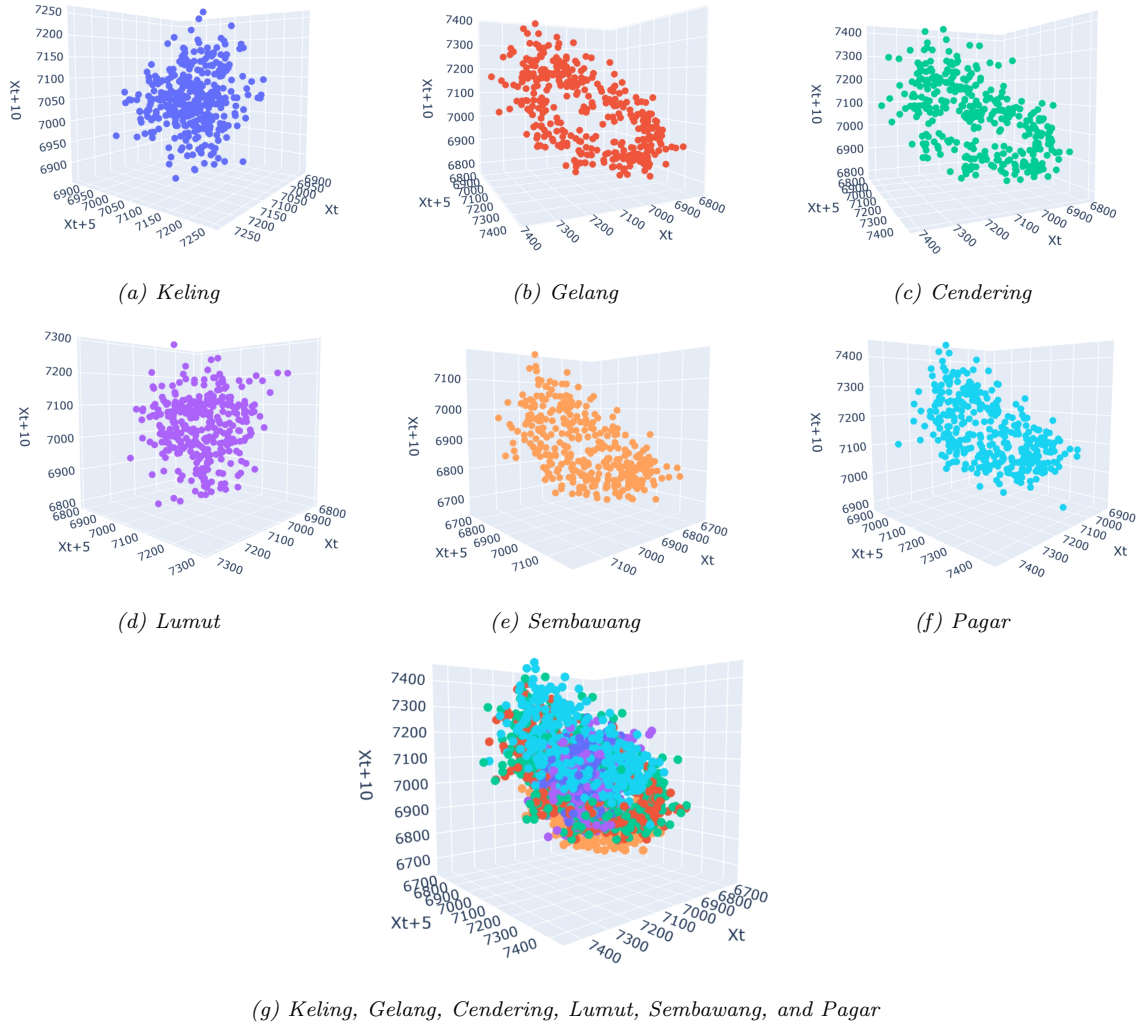


Figure 10: Six sets of point cloud data obtained from Takens' Embedding Theorem with dimension  $m = 3$  and delay  $\tau = 5$ .

### 45 3.1 Traditional $k$ -means/ $k$ -means++ Clustering

46 In this subsection, we evaluated the performance of a classifier based on traditional  $k$ -means/ $k$ -  
 47 means++ clustering for categorizing the six groups of point cloud data depicted in Figure 10.

48 To select the parameter  $k$  for our classifier, we considered that the data we obtained originated  
 49 from three sea regions of Peninsular Malaysia (western coast, east coast, and southern coast) and  
 50 comprised six distinct datasets. Therefore, we tested our classifier with parameter  $k$  in the range  
 51 of  $[3, 6]$ . Figure 11 illustrates the results of our classifier using traditional  $k$ -means clustering with  
 52 parameter  $k = 5$ . In this visualization, green squares represent the centroids of different classes  
 53 obtained by the classifier, while differently colored balls indicate the sets of point cloud data from  
 54 the six tide gauge stations as shown in Figure 10.

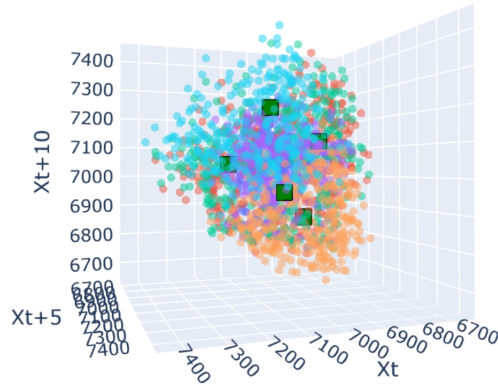


Figure 11:  $k$ -means clustering with  $k = 5$ .

55 The following four tables present the percentages of points from each set of point cloud data  
 56 being categorized into each class. Cells filled with a light red color indicate the value of  $P_i$  (as  
 57 defined in Eq.2), representing the highest percentage of a set of point cloud data being categorized  
 58 into a specific class. In Table 2, aside from Sembawang, which shows a credible probability of 0.982  
 59 for being categorized into Class 1, none of the other sets can be credibly categorized into the classes  
 60 with the highest probabilities shown. This pattern remains consistent across different selections of  
 61 the parameter  $k$ , as demonstrated in Table 3, Table 4, and Table 5. Referring to Figure 10, the  
 62 reason why the data set represented in orange (from Sembawang) can be credibly classified into  
 63 one class (with  $P_i$  exceeding 0.85 in most cases) is that for most orange balls, we can identify a  
 64 two-dimensional plane that separates them from the others, resulting in most orange balls being  
 65 closer to a particular centroid than others. This indicates that the  $k$ -means clustering classifier,  
 66 regardless of the choice of initial centroids, poorly categorizes data groups with high dispersion  
 67 that are mixed together. The poor performance of the traditional  $k$ -means/ $k$ -means++ classifier  
 68 foregrounds the need to consider improved methods.

Table 2:  $k$ -means clustering with  $k = 3$ .

	Class 1	Class 2	Class 3
Keling	0.040	0.398	0.561
Gelang	0.031	0.401	0.566
Cendering	0.008	0.402	0.590
Lumut	0.078	0.421	0.501
Sembawang	0.982	0.008	0.008
Pagar	0.000	0.392	0.507

Table 3: *k*-means clustering with *k* = 4.

	Class 1	Class 2	Class 3	Class 4
Keling	0.340	0.296	0.037	0.325
Gelang	0.337	0.331	0.000	0.331
Cendering	0.322	0.337	0.000	0.340
Lumut	0.290	0.311	0.063	0.334
Sembawang	0.011	0.008	0.968	0.011
Pagar	0.340	0.328	0.000	0.331

Table 4: *k*-means clustering with *k* = 5.

	Class 1	Class 2	Class 3	Class 4	Class 5
Keling	0.261	0.218	0.009	0.287	0.223
Gelang	0.328	0.008	0.000	0.325	0.337
Cendering	0.290	0.098	0.000	0.316	0.293
Lumut	0.273	0.145	0.0174	0.308	0.255
Sembawang	0.055	0.000	0.892	0.020	0.031
Pagar	0.056	0.610	0.000	0.023	0.098

Table 5: *k*-means clustering with *k* = 6.

	Class 1	Class 2	Class 3	Class 4	Class 5	Class 6
Keling	0.247	0.250	0.005	0.142	0.209	0.145
Gelang	0.250	0.308	0.000	0.284	0.055	0.101
Cendering	0.233	0.302	0.000	0.250	0.093	0.122
Lumut	0.279	0.267	0.008	0.194	0.162	0.087
Sembawang	0.069	0.020	0.840	0.0697	0.000	0.000
Pagar	0.020	0.229	0.000	0.020	0.395	0.334

69 **3.2 Results by the Hybrid Method for the Selected Six Datasets**

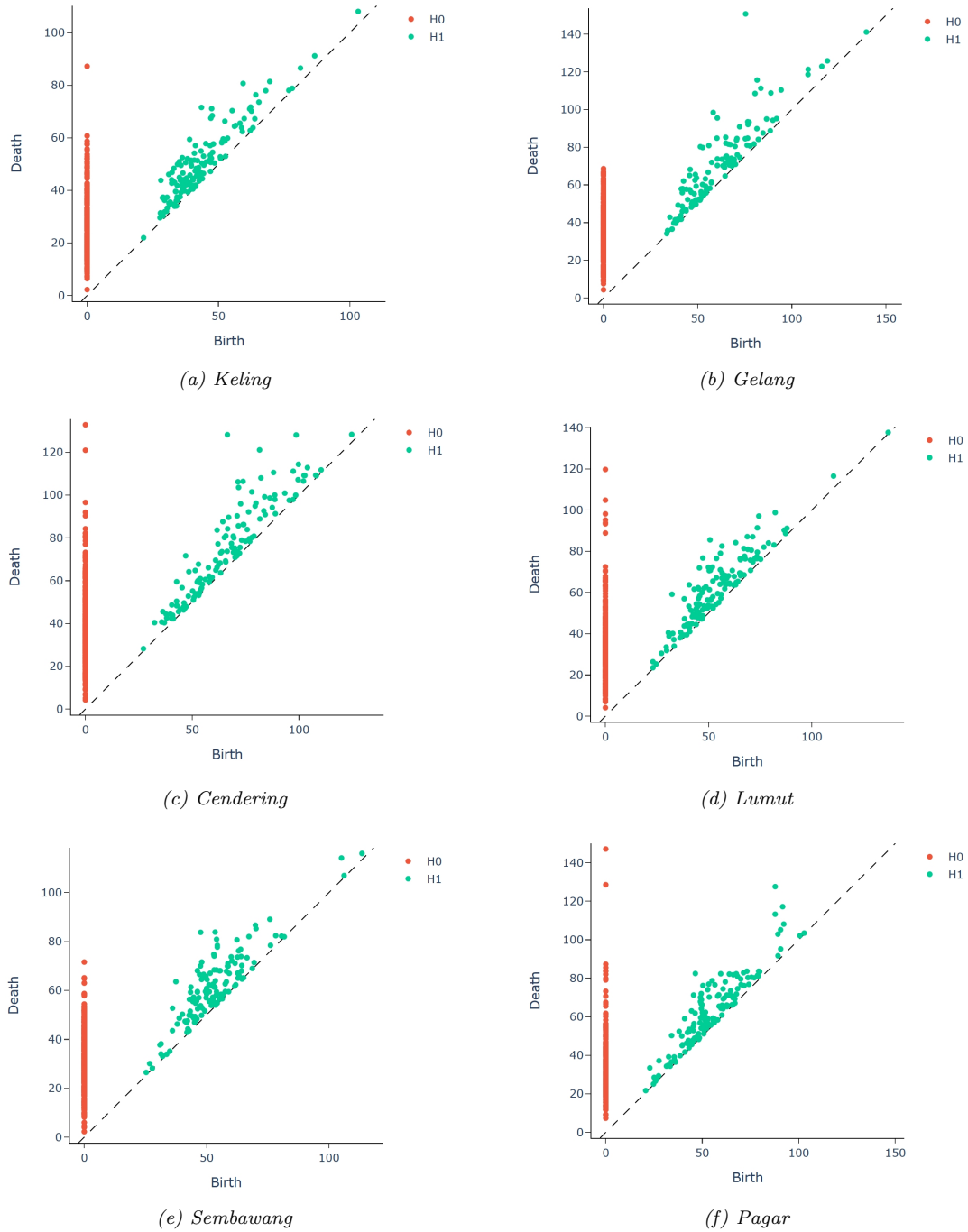


Figure 12: Persistence diagrams of six groups of point cloud data.

70 In this subsection, we assess the effectiveness of our proposed hybridization of  $k$ -means/ $k$ -means++  
 71 clustering and persistent homology (see details in Algorithm 1). Before applying  $k$ -means/ $k$ -  
 72 means++ clustering, we use persistent homology to quantify the shapes of each set of point cloud  
 73 data obtained from the embedding theorem (as shown in Figure 10). This analysis involves deter-

74 mining the shapes of the data groups using the maximum  $H_1$  lifetime (as shown in Table 6), which  
75 represents a prominent shape-based feature of the dataset. We visualize the results of persistent  
76 homology in Figure 12 and its subfigures, where the  $x$ -axis denotes the birth time of  $H_0$  and  $H_1$ ,  
77 and the  $y$ -axis denotes their death times. This computation allows us to distinguish between data  
78 shapes and use this information as a prior for our subsequent analysis of classes using  $k$ -means++  
79 clustering. It’s important to note that the overlapping names of classes in different tables (e.g.,  
80 Class 1 in Table 7 and Table 8) are for simplification purposes and do not imply that they carry  
81 the same physical meaning. In fact, we do not attribute any specific physical meaning to individual  
82 classes, as discussed in the earlier section. The result shown in Table 6 is highly consistent with  
83 the locations and Monsoon patterns in Malaysia: Cendering and Glang are exposed prominently  
84 to Nov-March Northeast Monsoon, while other four tide gauge stations are exposed to April-Sept  
85 Southwest Monsoon. The results of persistent homology provide valuable insights. For instance,  
86 Keling, Lumut, Sembawang, and Pagar, which have similar maximum  $H_1$  lifetimes, share similar  
87 shapes. The shapes of sets inferred from them provided crucial prior information. Therefore,  
88 armed with this prior shape information, we proceed to run  $k$ -means++ clustering on these four  
89 groups. The results are presented in Figure 13 and Table 7. Unlike the results shown in Table 2 to  
90 Table 5, Table 7 reveals that Sembawang and Pagar can be credibly categorized into Class 3 with  
91 the highest probability of 0.820 and Class 1 with the highest probability of 0.917, respectively.  
92 Figure 13 further demonstrates the improved performance of the  $k$ -means++ clustering classifier.  
93 Therefore, Sembawang and Pagar likely have different patterns of sea level variability and can be  
94 categorized into two distinct classes using our proposed method. Additionally, as shown in Figure  
95 14 and Table 8, when we apply  $k$ -means clustering to Keling and Lumut, they are categorized into  
96 a single class distinct from Sembawang and Pagar.

Table 6: Maximum lifetimes obtained from embedded point data groups of the study locations.

Location	Maximum lifetime	Coastal Region	Dominated Monsoon
Cendering	62.731	East	Nov-March Northeast Monsoon
Gelang	74.541	East	
Lumut	34.860	West	April-Sept Southwest Monsoon
Keling	34.911	West	
Sembawang	36.162	Southern	
Pagar	36.521	Southern	

Table 7: A resulted table from applying *k*-means clustering algorithm to the sea level data from Keling, Lumut, Sembawang and Pagar.

	Class 1	Class 2	Class 3
Keling	0.308	0.680	0.011
Lumut	0.297	0.663	0.04
Sembawang	0.000	0.180	0.820
Pagar	0.917	0.083	0.000

Table 8: A resulted table from applying *k*-means clustering algorithm to the sea level data from Keling and Lumut.

	Class 1	Class 2
Keling	0.540	0.460
Lumut	0.462	0.537

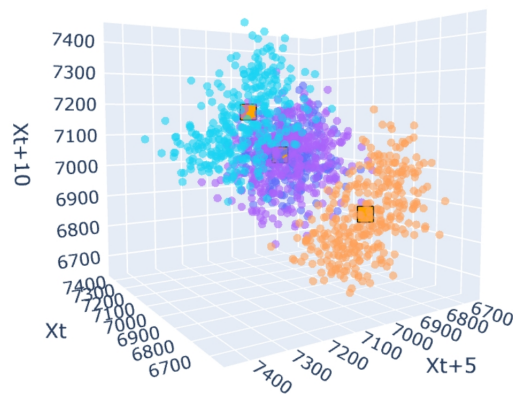


Figure 13: A resulted figure from applying *k*-means clustering algorithm to the sea level data from Keling, Lumut, Sembawang and Pagar.

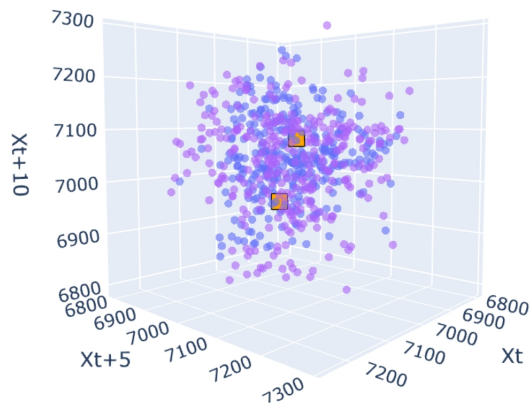


Figure 14: A resulted figure from applying *k*-means clustering algorithm to the sea level data from Keling and Lumut.

Table 9:  $k$ -means clustering run for Cendering and Gelang.

	Class 1	Class 2
Gelang	0.497	0.503
Cendering	0.521	0.479

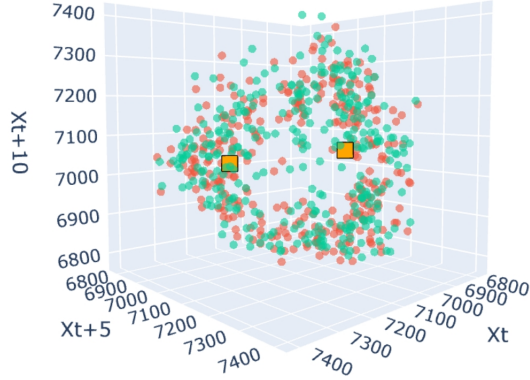


Figure 15:  $k$ -means clustering run for Cendering and Gelang.

97 Secondly, Cendering and Gelang exhibit a similar shape distinct from the other four tide gauge  
 98 stations. We apply  $k$ -means clustering to these two stations, and the result, presented in Table 11  
 99 and Figure 15, shows that Cendering and Gelang are classified into the same category. In the next  
 100 section, we will provide a detailed explanation and discussion of these results, drawing insights  
 101 from ocean science and mathematical statistics.

### 102 3.3 Results by the Hybrid Method for Fourteen Datasets

Table 10:  $k$ -means clustering run for Langkawi, Pinang, and Tioman that share the similar shapes determined by persistent homology.

	Class 1	Class 2
Langkawi	0.250	0.750
Pinang	0.852	0.148
Tioman	0.264	0.735

103 In this subsection, we have omitted some technical details that are similar to those presented  
 104 in Section 3.2. The methodology flow and the tables or figures used in this subsection are all  
 105 analogous to those found in the previous subsection. One difference is that we had fixed the  
 106 dimension to  $m = 3$  and the time delay to  $\tau = 8$ , as the optimal time delay varies significantly  
 107 across the fourteen datasets. The application of persistent homology to fourteen datasets from  
 108 fourteen different tide gauge stations revealed four groups, each exhibiting a similar shape. The

109 first group includes Langkawi, Pinang, and Tioman, and the results of the  $k$ -means clustering for  
 110 them are shown in Table 10 and Figure 16. This analysis indicated that Langkawi and Tioman  
 111 share a similar pattern of sea level variability, distinct from that of Pinang. The second group  
 112 comprises Geting, Cendering, and Gelang, as shown in Table 11 and Figure 17, and the results  
 113 suggest that Geting, Cendering, and Gelang exhibit a similar pattern of sea level variability.

114 The third group comprises Lumut, Kelang, Keling, Kukup, and Shoal, as shown in Table 12 and  
 115 Figure 18. The analysis revealed that Lumut, Kelang, Keling, and Shoal share a similar pattern of  
 116 sea level variability, distinct from that of Kukup. The fourth group consists of Sedili, Sembawang,  
 117 and Pagar, as shown in Table 13 and Figure 19. Our findings indicate that these three regions  
 118 exhibit different patterns of sea level rise and fall.

119 We summarized our results in figures of Figure 20. In these figures, differently colored arrows  
 120 and letters represent different patterns of sea level variability. For instance, according to our  
 121 approach, Lumut, Kelang, Keling, and Shoal share a similar pattern of sea level variability, so they  
 122 are all indicated by red arrows and letters in figures of Figure 20. We showed the specific position  
 123 and categories in Figure 20.

Table 11:  $k$ -means clustering run for Geting, Cendering, and Gelang that share the similar shapes determined by persistent homology.

	Class 1	Class 2	Class 3
Geting	0.334	0.329	0.337
Cendering	0.328	0.337	0.334
Gelang	0.331	0.328	0.340

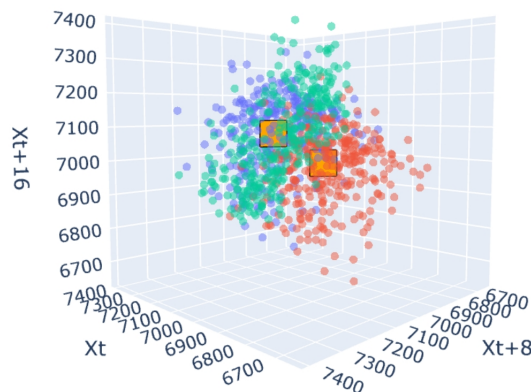


Figure 16: The figure shows data points for the first group (lavender indicates Langkawai, red indicates Pulau Pinang, and green indicates Tioman) and the generated centroids of different classes colored by orange.

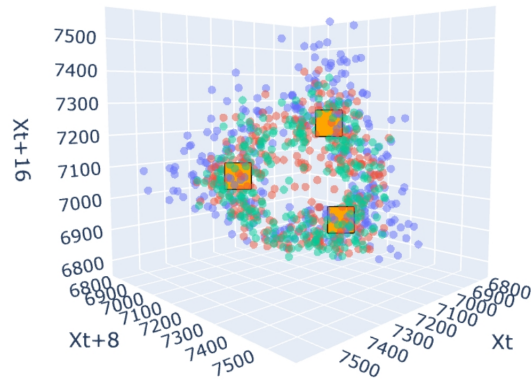


Figure 17: The figure shows data points for the second group (lavender indicates Geting, red indicates Cendering, and green indicates Gelang) and the generated centroids of different classes colored by orange squares.

Table 12:  $k$ -means clustering run for Lumut, Kelang, Keling, Kukup, and Shoal that share the similar shapes determined by persistent homology.

	Class 1	Class 2	Class 3	Class 4
Lumut	0.293	0.255	0.258	0.191
Kelang	0.255	0.128	0.044	0.572
Keling	0.270	0.209	0.363	0.157
Kukup	0.148	0.140	0.706	0.058
Shoal	0.299	0.177	0.297	0.227

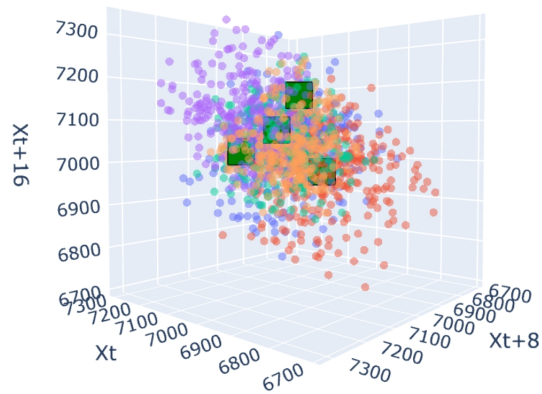


Figure 18: This figure shows data points for the third group (lavender indicates Lumut, red indicates Kelang, green indicates Keling, and purple indicates Kukup, and orange indicates Shoal) and the generated centroids of different classes colored by green squares.

Table 13:  $k$ -means clustering run for Sedili, Sembawang, and Pagar that share the similar shapes determined by persistent homology.

	Class 1	Class 2	Class 3
Sedili	0.000	0.195	0.805
Sembawang	0.901	0.000	0.098
Pagar	0.000	0.674	0.325

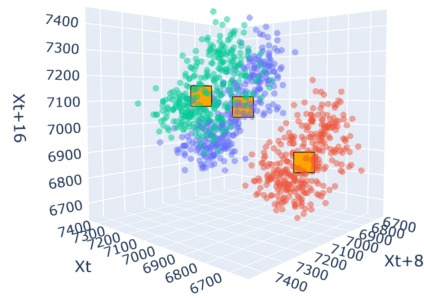
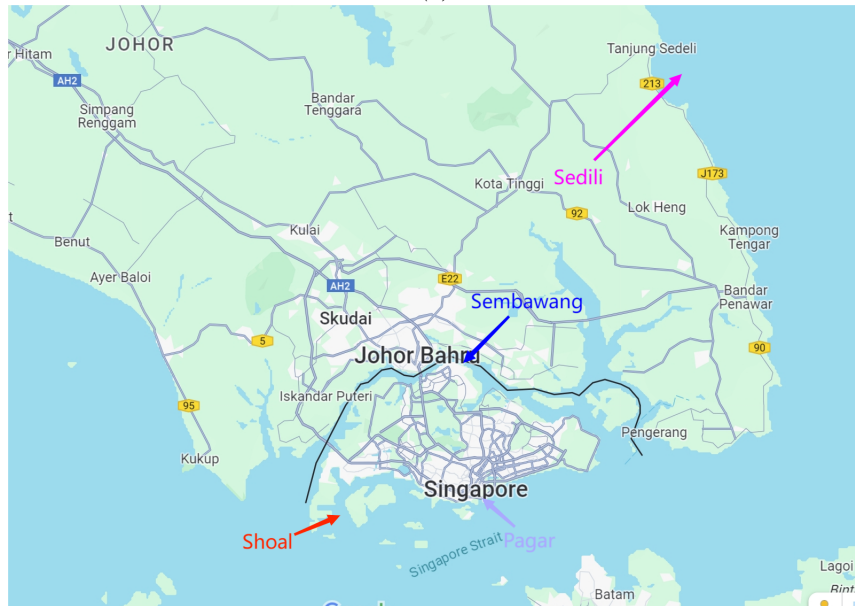


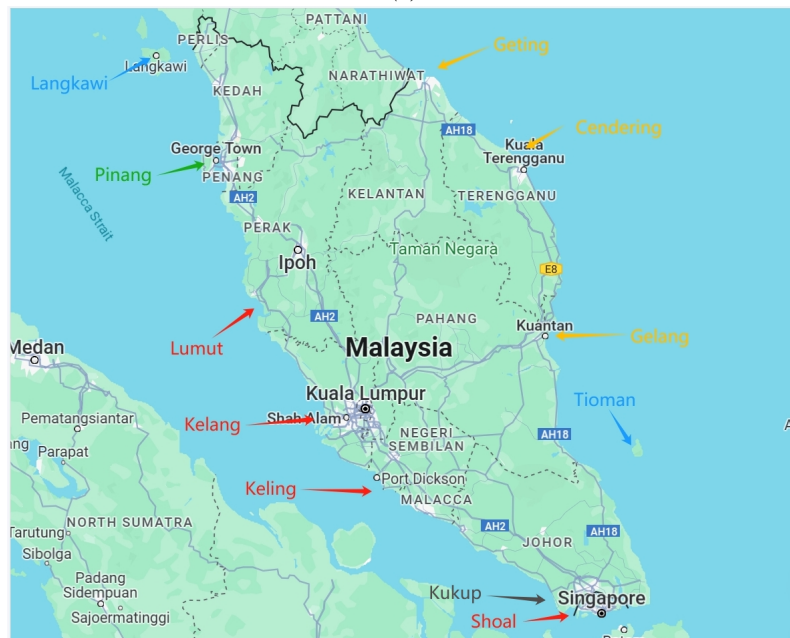
Figure 19: This figure shows data points for the fourth group (lavender indicates Sedili, red indicates Sembawang, and green indicates Pagar) and the generated centroids of different classes colored by orange squares.

Category1	Cat.2	Cat.3	Cat.4	Cat.5	Cat.6	Cat.7	Cat.8
Langkawi	Pinang	Lumut	Geting	Kukup	Sedili	Sembawang	Pagar
Tioman		Kelang	Cendering				
		Keling	Gelang				
		Shoal					

(a)



(b)



(c)

Figure 20: This figure shows the final categorization of fourteen tide gauge stations into eight categories. The figure (a) shows the final categorization and stations contained in each class. The two maps, shown in figure (b) and (c), below show specific locations of the stations. Different categories are colored differently in the figures.



Figure 21: This figure shows parts of islands or shorelines in which fourteen tide gauge stations are located, the position of tide station is indicted by green arrow, and name is shown as the caption of corresponding subfigure.

## 124 4 Discussions

### 125 4.1 Discussions of Results for the Six Selected Datasets

126 The results obtained by applying the hybridization of  $k$ -means/ $k$ -means++ clustering and per-  
127 sistent homology (Algorithm 1) align with our initial expectations. We identified four distinct  
128 classes of sea level variability patterns across three sea regions: Keling, Gelang, Cendering, Lumut,  
129 Sembawang, and Pagar.

130 Notably, the sea regions on the east coast were categorized into a single class, which corresponds  
131 well with real-world conditions. Peninsular Malaysia is located at the center of the Sunda Shelf,  
132 bordered to the east by the South China Sea, the largest marginal sea in the Pacific Basin, and to  
133 the west by the Andaman Sea of the Indian Ocean (see Figure 22). The sea regions along the east  
134 coast face the South China Sea, where weather patterns and ocean currents are predominantly  
135 influenced by the Asian monsoonal wind. This wind system branches into two major parts: the  
136 East Asian–western Pacific monsoon and the South Asian–Indian monsoon (see more details in  
137 [43], [44], [45], [46], [47]). Consequently, sea level variability along the east coast of Peninsular  
138 Malaysia are significantly affected by the Asian Monsoon.

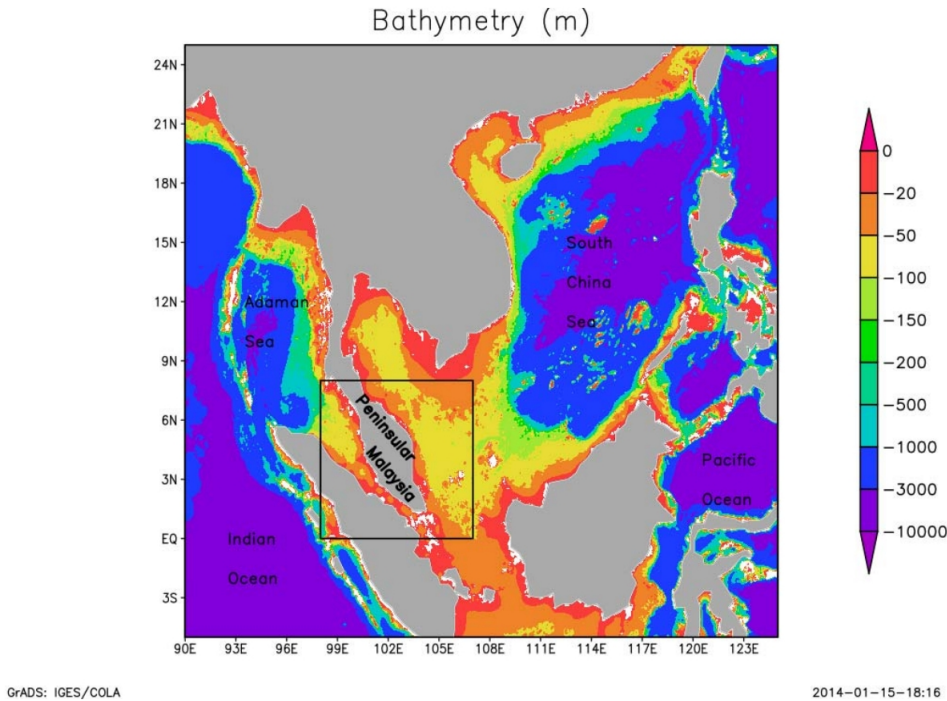


Figure 22: Bathymetry in the region with the black box indicating area of interest [4].

139 In contrast, sea regions on the west coast are situated in the Strait of Malacca, which receives

140 less influence from the Asian monsoonal wind due to the protection provided by the landmass of  
 141 Peninsular Malaysia [4]. These regions are adjacent to the Bay of Bengal and the Andaman Sea,  
 142 where sea level anomalies are induced by the Indian Ocean Dipole. Also, sea level variability in  
 143 the Malacca Strait show a strong correlation with the ENSO index [4]. While sea level variability  
 144 on both the east and west coasts of Peninsular Malaysia is somewhat synchronized with the El  
 145 Niño-Southern Oscillation (ENSO) ([48], [49], [50]), variations induced by the Indian Ocean Dipole  
 146 primarily affect the west coast. Our hybridized approach (Algorithm 1) did grouped Lumut and  
 147 Keling, the sea regions along the west coast, into one class, indicating that they have the similar  
 148 pattern of sea level variability, while Cendering and Cendering in the east coast into another class.

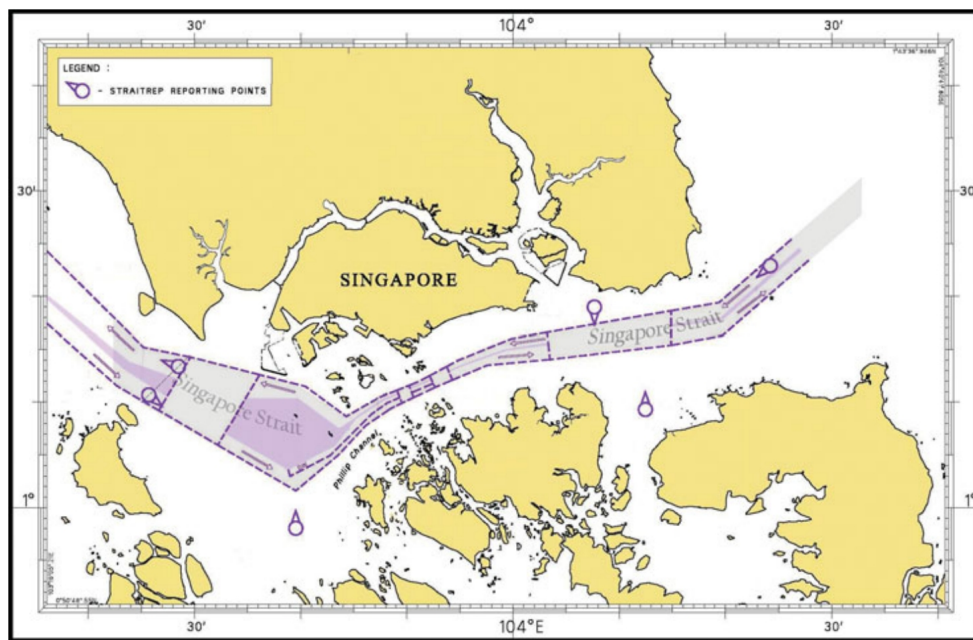


Figure 23: Singapore Strait [51].

149 In addition, despite Pagar and Sembawang having similar latitudes and longitudes as shown  
 150 in Table 1, our findings revealed distinct patterns in their sea level variability. This discrepancy  
 151 aligns with their geographical and locational differences. Pagar is situated in the Singapore Strait  
 152 (refer to Figure 23). While the sea level variability of Pagar is also influenced by ENSO to some  
 153 extent, other local phenomena and factors at various scales may play more significant roles ([52]).  
 154 For instance, extensive coastal development by the local government (Singapore, as a small island  
 155 nation, has been reclaiming land from the sea to expand its territory) greatly impacts local sea  
 156 level variability [53]. We did identify a different pattern of sea level variability for Pagar located  
 157 in Singapore Strait.

158 Besides, Sembawang locates between landmasses and the sea level variability of it is more  
 159 sensitive to inland factors like urban development [53] or transportation. Our results assigned it a

160 class different from Pagar.

## 161 4.2 Discussions of Results for the Fourteen Datasets

162 The interpretation of the results for the fourteen datasets is complex due to a wide range of  
163 influencing factors. Numerous factors impact sea level variability at each tide gauge station,  
164 making it intricate to decipher. Despite this complexity, our findings unveiled a coastal and  
165 spatial coherence, grouping stations along the east coast, west coast, and southern region. For  
166 instance, stations like Geting, Cendering, and Gelang, situated along the east coast with close  
167 longitudes and latitudes, exhibited similar patterns of sea level variability according to our results.  
168 Another example is the grouping of stations including Lumut, Kelang, Keling, and Shoal, which  
169 also displayed coherent patterns. However, there are some interesting and unexpected deviations  
170 from our initial hypothesis. The pattern of sea level variability in Langkawi is more similar to  
171 that of Tioman than to Pinang, despite Pinang's closer proximity to Langkawi and its location  
172 on the same coast as Langkawi. Several factors may contribute to this difference. One factor to  
173 consider is that the proximity of islands at a distance from the mainland may result in similar ocean  
174 currents around Langkawi and Tioman [54]. Another factor to consider could be the intensity of  
175 human activities. For example, studies have shown that extensive tourism has led to significant  
176 alterations in the coastal resorts of Tioman and Langkawi (see more details in [55], [56], [57]).  
177 An additional interesting result is that Kukup was not grouped with Lumut, Kelang, Keling,  
178 and Shoal, despite their locations along the west coast in the narrow part of the Malacca Strait.  
179 Moreover, despite Shoal and Pagar being closer to the Singapore Strait, our results showed that  
180 they exhibited different patterns of sea level variability. Sedili, despite its location along the west  
181 coast, was initially grouped with Sembawang or Pagar based on the shape information provided by  
182 the homology group. However, it has been categorized into different patterns of sea level variability  
183 eventually by  $k$ -means clustering. This could be explained by both the proximity of Sedili to  
184 Singapore Strait and its location whose current pattern and temperature pattern is predominantly  
185 influenced by the South China Sea [58].

186 These intriguing results, which pose a more challenging interpretation due to the need to  
187 consider a broad range of factors, point toward the direction of future research. One potential  
188 approach could involve utilizing Path Homology [59] or Discrete Morse Matching [60] to analyze  
189 the differences in ocean currents in these regions and draw credible conclusions.

## 190 5 Conclusions

191 The paper investigated the hybridization of persistent homology, a technique from topological data  
192 analysis, with the widely-used  $k$ -means/ $k$ -means++ clustering method. The study demonstrated  
193 that this hybrid approach, presented as Algorithm 1, significantly enhances clustering performance  
194 when applied to time-series sea level data spanning January 1989 to December 2018 from fourteen  
195 regions of Peninsular Malaysia. The method involves utilizing Taken’s embedding theorem and  
196 persistent homology in conjunction with traditional clustering.

197 The process of the proposed approach begins with the determination of a suitable time delay  
198 using the false nearest neighbors criterion, resulting in groups of point cloud data. Subsequently, the  
199 shape of each group is determined using persistent homology, providing a prior for the traditional  
200 clustering in the third step. In the third step, we ran  $k$ -means clustering algorithm for groups  
201 sharing the same or similar shapes and determined their final categories. The approach has several  
202 strengths. Firstly, it does not rely on pre-assumed models for the time-series data. Secondly, it  
203 is versatile and applicable to various types of sea level time-series data. Lastly, it outperforms  
204 traditional clustering methods in terms of performance.

205 For the selected six sea regions, our results yielded several key and interesting insights. Firstly,  
206 the classification of Cendering and Gelang into the same cluster reflects the influence of the Asian  
207 monsoonal wind on sea regions along the east coast facing the South China Sea. Secondly, the  
208 grouping of Lumut and Keling is attributed to their location in the Strait of Malacca, which expe-  
209 riences less influence from the Asian monsoonal wind due to the protection offered by Peninsular  
210 Malaysia. These regions are adjacent to the Bay of Bengal and the Andaman Sea, where sea level  
211 anomalies are influenced by the Indian Ocean Dipole. Additionally, despite their proximity in lon-  
212 gitude and latitude, Sembawang and Pagar exhibit different sea level variability patterns, which  
213 align with their geographical differences. Pagar, situated in the Singapore Strait, is influenced  
214 by various local phenomena and factors, while Sembawang, located between landmasses, is more  
215 sensitive to inland factors like urban development and transportation. Interpreting the results for  
216 all fourteen sea regions presents a considerable challenge. Despite the numerous factors influencing  
217 and complicating sea level variability among these regions, our findings revealed a coastal and  
218 spatial coherence across the studied sea regions. Exceptions could be further explained by future  
219 research, which might rely on graph-related homology methods like Path Homology, Discrete Morse  
220 Theory, or the Mapper Algorithm [61].

221 Our approach contributes to sea level change predictions by leveraging historical data for accu-  
222 rate forecasts, particularly in data-rich regions, or the development of effective prediction models

223 incorporating topological features of data sets. These predictions can then guide forecasts in  
224 less-documented areas if similar sea level trends are observed. Additionally, we highlight the sig-  
225 nificance of location in machine learning analyses of sea level variations. This emphasizes the need  
226 for models to heavily weight location due to its impact on sea level patterns.

## 227 **References**

- 228 [1] G. A. Meehl, W. M. Washington, W. D. Collins, J. M. Arblaster, A. Hu, L. E. Buja, W. G.  
229 Strand, and H. Teng, “How much more global warming and sea level rise?” *science*, vol. 307,  
230 no. 5716, pp. 1769–1772, 2005.
- 231 [2] A. Cazenave and W. Llovel, “Contemporary sea level rise,” *Annual review of marine science*,  
232 vol. 2, pp. 145–173, 2010.
- 233 [3] D. J. Mallinson, S. J. Culver, D. R. Corbett, P. R. Parham, N. A. M. Shazili, and R. Yaacob,  
234 “Holocene coastal response to monsoons and relative sea-level changes in northeast peninsular  
235 malaysia,” *Journal of Asian Earth Sciences*, vol. 91, pp. 194–205, 2014.
- 236 [4] Q. Luu, P. Tkalich, and T. Tay, “Sea level trend and variability around peninsular malaysia,”  
237 *Ocean Science*, vol. 11, no. 4, pp. 617–628, 2015.
- 238 [5] S. Mohan and P. Vethamony, “Interannual and long-term sea level variability in the eastern  
239 indian ocean and south china sea,” *Climate Dynamics*, vol. 50, pp. 3195–3217, 2018.
- 240 [6] M. G. Scotto, A. M. Alonso, and S. M. Barbosa, “Clustering time series of sea levels: Extreme  
241 value approach,” *Journal of waterway, port, coastal, and ocean engineering*, vol. 136, no. 4,  
242 pp. 215–225, 2010.
- 243 [7] M. Imani, R.-J. You, and C.-Y. Kuo, “Forecasting caspian sea level changes using satellite  
244 altimetry data (june 1992–december 2013) based on evolutionary support vector regression  
245 algorithms and gene expression programming,” *Global and planetary change*, vol. 121, pp.  
246 53–63, 2014.
- 247 [8] C. Song, X. Chen, X. Ding, and L. Zhang, “Sea level simulation with signal decomposition  
248 and machine learning,” *Ocean Engineering*, vol. 241, p. 110109, 2021.
- 249 [9] J. P. den Bieman, M. P. de Ridder, M. I. Mata, and J. C. van Nieuwkoop, “Hybrid modelling to  
250 improve operational wave forecasts by combining process-based and machine learning models,”  
251 *Applied Ocean Research*, vol. 136, p. 103583, 2023.

- 252 [10] H. Jiang, H. Wang, M. A. Vaz, and X. Bai, “Research on dynamic response prediction of  
253 semi-submersible wind turbine platform in real sea test model based on machine learning,”  
254 *Applied Ocean Research*, vol. 142, p. 103808, 2024.
- 255 [11] M. Scotto, S. M. Barbosa, and A. M. Alonso, “Model-based clustering of baltic sea-level,”  
256 *Applied Ocean Research*, vol. 31, no. 1, pp. 4–11, 2009.
- 257 [12] V. Nieves, C. Radin, and G. Camps-Valls, “Predicting regional coastal sea level changes with  
258 machine learning,” *Scientific Reports*, vol. 11, no. 1, p. 7650, 2021.
- 259 [13] P. S. Bradley, K. P. Bennett, and A. Demiriz, “Constrained k-means clustering,” *Microsoft*  
260 *Research, Redmond*, vol. 20, no. 0, p. 0, 2000.
- 261 [14] D. T. Pham, S. S. Dimov, and C. D. Nguyen, “Selection of k in k-means clustering,” *Proceed-*  
262 *ings of the Institution of Mechanical Engineers, Part C: Journal of Mechanical Engineering*  
263 *Science*, vol. 219, no. 1, pp. 103–119, 2005.
- 264 [15] L. Wasserman, “Topological data analysis,” *Annual Review of Statistics and Its Application*,  
265 vol. 5, pp. 501–532, 2018.
- 266 [16] N. Otter, M. A. Porter, U. Tillmann, P. Grindrod, and H. A. Harrington, “A roadmap for the  
267 computation of persistent homology,” *EPJ Data Science*, vol. 6, pp. 1–38, 2017.
- 268 [17] T. K. Dey and Y. Wang, *Computational topology for data analysis*. Cambridge University  
269 Press, 2022.
- 270 [18] G. Favelier, C. Gueunet, A. Gyulassy, J. Kitware, J. Levine, J. Lukasczyk, D. Sakurai,  
271 M. Soler, J. Tierny, W. Usher *et al.*, “Topological data analysis made easy with the topology  
272 toolkit,” *arXiv preprint arXiv:1806.08126*, 2018.
- 273 [19] L. M. Seversky, S. Davis, and M. Berger, “On time-series topological data analysis: New data  
274 and opportunities,” in *Proceedings of the IEEE conference on computer vision and pattern*  
275 *recognition workshops*, 2016, pp. 59–67.
- 276 [20] N. F. S. Zulkepli, M. S. M. Noorani, F. A. Razak, M. Ismail, and M. A. Alias, “Hybridization of  
277 hierarchical clustering with persistent homology in assessing haze episodes between air quality  
278 monitoring stations,” *Journal of environmental management*, vol. 306, p. 114434, 2022.
- 279 [21] R. Gobithaasan, K. D. Selvarajh, and K. T. Miura, “Clustering datasaurus dozen using bot-  
280 tleneck distance, wasserstein distance (wd) and persistence landscapes,” *Journal of Advanced*  
281 *Research in Applied Sciences and Engineering Technology*, vol. 38, no. 1, pp. 12–24, 2024.

- 282 [22] A. Hallam, “A review of the broad pattern of jurassic sea-level changes and their possible  
283 causes in the light of current knowledge,” *Palaeogeography, Palaeoclimatology, Palaeoecology*,  
284 vol. 167, no. 1-2, pp. 23–37, 2001.
- 285 [23] R. Gobithaasan, Z. A. Hasan, K. D. Selvarajh, K.-S. Wong, S. Mamat, M. Z. Muhamad Ali,  
286 K. T. Miura, and P. Dotko, “Clustering selected terengganu’s rainfall stations based on per-  
287 sistent homology,” *Thai Journal of Mathematics*, pp. 197–211, 2022.
- 288 [24] Z. A. Hasan, R. Gobithaasan, N. F. S. M. Zulkepli, M. Z. M. Ali, K. T. Miura, and P. Dłotko,  
289 “Identifying irregular rainfall patterns using persistent homology,” *Journal of Advanced Re-  
290 search in Applied Sciences and Engineering Technology*, vol. 35, no. 1, pp. 26–36, 2024.
- 291 [25] P. R. Thompson and M. A. Merrifield, “A unique asymmetry in the pattern of recent sea level  
292 change,” *Geophysical Research Letters*, vol. 41, no. 21, pp. 7675–7683, 2014.
- 293 [26] J. A. Church, N. J. White, R. Coleman, K. Lambeck, and J. X. Mitrovica, “Estimates of the  
294 regional distribution of sea level rise over the 1950–2000 period,” *Journal of climate*, vol. 17,  
295 no. 13, pp. 2609–2625, 2004.
- 296 [27] M. Ryo and M. C. Rillig, “Statistically reinforced machine learning for nonlinear patterns and  
297 variable interactions,” *Ecosphere*, vol. 8, no. 11, p. e01976, 2017.
- 298 [28] S. J. Holgate, A. Matthews, P. L. Woodworth, L. J. Rickards, M. E. Tamisiea, E. Bradshaw,  
299 P. R. Foden, K. M. Gordon, S. Jevrejeva, and J. Pugh, “New data systems and products at  
300 the permanent service for mean sea level,” *Journal of Coastal Research*, vol. 29, no. 3, pp.  
301 493–504, 2013.
- 302 [29] I. C. Abazu, A. H. M. Din, and K. M. Omar, “Mean dynamic topography over peninsular  
303 malaysian seas using multimission satellite altimetry,” *Journal of Applied Remote Sensing*,  
304 vol. 11, no. 2, pp. 026 017–026 017, 2017.
- 305 [30] S. B. Taieb, A. Sorjamaa, and G. Bontempi, “Multiple-output modeling for multi-step-ahead  
306 time series forecasting,” *Neurocomputing*, vol. 73, no. 10-12, pp. 1950–1957, 2010.
- 307 [31] Z. Bankó and J. Abonyi, “Correlation based dynamic time warping of multivariate time series,”  
308 *Expert Systems with Applications*, vol. 39, no. 17, pp. 12 814–12 823, 2012.
- 309 [32] Y. Gutman, Y. Qiao, and G. Szabó, “The embedding problem in topological dynamics and  
310 takens’ theorem,” *Nonlinearity*, vol. 31, no. 2, p. 597, 2018.

- 311 [33] T. M. Kodinariya, P. R. Makwana *et al.*, “Review on determining number of cluster in k-means  
312 clustering,” *International Journal*, vol. 1, no. 6, pp. 90–95, 2013.
- 313 [34] S. E. Y. Nayini, S. Geravand, and A. Maroosi, “A novel threshold-based clustering method  
314 to solve k-means weaknesses,” in *2017 International Conference on Energy, Communication,  
315 Data Analytics and Soft Computing (ICECDS)*. IEEE, 2017, pp. 47–52.
- 316 [35] R. Ghrist, “Barcodes: the persistent topology of data,” *Bulletin of the American Mathematical  
317 Society*, vol. 45, no. 1, pp. 61–75, 2008.
- 318 [36] M. Johnson and J.-H. Jung, “Instability of the betti sequence for persistent homology and a  
319 stabilized version of the betti sequence,” *arXiv preprint arXiv:2109.09218*, 2021.
- 320 [37] P. Bubenik, M. Hull, D. Patel, and B. Whittle, “Persistent homology detects curvature,”  
321 *Inverse Problems*, vol. 36, no. 2, p. 025008, 2020.
- 322 [38] R. Turkes, G. F. Montufar, and N. Otter, “On the effectiveness of persistent homology,”  
323 *Advances in Neural Information Processing Systems*, vol. 35, pp. 35 432–35 448, 2022.
- 324 [39] P. Virtanen, R. Gommers, T. E. Oliphant, M. Haberland, T. Reddy, D. Cournapeau,  
325 E. Burovski, P. Peterson, W. Weckesser, J. Bright *et al.*, “Scipy 1.0: fundamental algorithms  
326 for scientific computing in python,” *Nature methods*, vol. 17, no. 3, pp. 261–272, 2020.
- 327 [40] G. Tauzin, U. Lupo, L. Tunstall, J. B. Pérez, M. Caorsi, A. M. Medina-Mardones, A. Dassatti,  
328 and K. Hess, “giotto-tda: A topological data analysis toolkit for machine learning and data  
329 exploration,” *The Journal of Machine Learning Research*, vol. 22, no. 1, pp. 1834–1839, 2021.
- 330 [41] Y. Umeda, “Time series classification via topological data analysis,” *Information and Media  
331 Technologies*, vol. 12, pp. 228–239, 2017.
- 332 [42] C. Wong, R. Venneker, S. Uhlenbrook, A. Jamil, and Y. Zhou, “Variability of rainfall in  
333 peninsular malaysia,” *Hydrology and Earth System Sciences Discussions*, vol. 6, no. 4, pp.  
334 5471–5503, 2009.
- 335 [43] K. Wyrтки, *Physical oceanography of the Southeast Asian waters*. University of California,  
336 Scripps Institution of Oceanography, 1961, vol. 2.
- 337 [44] P. A. Hesp, C. C. Hung, M. Hilton, C. L. Ming, and I. M. Turner, “A first tentative holocene  
338 sea-level curve for singapore,” *Journal of Coastal Research*, pp. 308–314, 1998.
- 339 [45] D. Yihui and J. C. Chan, “The east asian summer monsoon: an overview,” *Meteorology and  
340 Atmospheric Physics*, vol. 89, no. 1-4, pp. 117–142, 2005.

- 341 [46] X. Huang, L. Huang, Y. Li, Z. Xu, C. Fong, D. Huang, Q. Han, H. Huang, Y. Tan, and S. Liu,  
342 “Main seagrass beds and threats to their habitats in the coastal sea of south china,” *Chinese*  
343 *Science Bulletin*, vol. 51, pp. 136–142, 2006.
- 344 [47] P. Wignall, S. Védérine, D. Bond, W. Wang, X.-L. Lai, J. Ali, and H.-S. Jiang, “Facies analysis  
345 and sea-level change at the guadalupian–lopingian global stratotype (laibin, south china), and  
346 its bearing on the end-guadalupian mass extinction,” *Journal of the Geological Society*, vol.  
347 166, no. 4, pp. 655–666, 2009.
- 348 [48] S. Aparna, J. McCreary, D. Shankar, and P. Vinayachandran, “Signatures of indian ocean  
349 dipole and el niño–southern oscillation events in sea level variations in the bay of bengal,”  
350 *Journal of Geophysical Research: Oceans*, vol. 117, no. C10, 2012.
- 351 [49] P. Sreenivas, C. Gnanaseelan, and K. Prasad, “Influence of el niño and indian ocean dipole on  
352 sea level variability in the bay of bengal,” *Global and Planetary Change*, vol. 80, pp. 215–225,  
353 2012.
- 354 [50] P. Tkalich, P. Vethamony, M. Babu, and P. Malanotte-Rizzoli, “Storm surges in the singapore  
355 strait due to winds in the south china sea,” *Natural hazards*, vol. 66, pp. 1345–1362, 2013.
- 356 [51] J. Weng, Q. Meng, and X. Qu, “Vessel collision frequency estimation in the singapore strait,”  
357 *The Journal of Navigation*, vol. 65, no. 2, pp. 207–221, 2012.
- 358 [52] P. Tkalich, P. Vethamony, Q.-H. Luu, and M. Babu, “Sea level trend and variability in the  
359 singapore strait,” *Ocean Science*, vol. 9, no. 2, pp. 293–300, 2013.
- 360 [53] T. Shaw, S. Chua, J. Majewski, L. Tanghua, D. Samanta, R. Kopp, and B. Horton, “Past,  
361 present and future sea levels in singapore,” in *EGU General Assembly Conference Abstracts*,  
362 2021, pp. EGU21–10 615.
- 363 [54] J. Watson, C. Hays, P. Raimondi, S. Mitarai, C. Dong, J. McWilliams, C. Blanchette,  
364 J. Caselle, and D. Siegel, “Currents connecting communities: nearshore community similarity  
365 and ocean circulation,” *Ecology*, vol. 92, no. 6, pp. 1193–1200, 2011.
- 366 [55] M. Mazlin, F. A. Minhaz, K. E. Lee, A. Lubna, C. T. Goh, E. Rahmah, T. Jamil, and A. K. H.  
367 Wong, “Achieving sustainable coastal environment in langkawi, malaysia,” *Borneo Journal of*  
368 *Marine Science and Aquaculture*, vol. 1, 2017.
- 369 [56] S. I. Omar, A. G. Othman, B. Mohamed, and A. Bahaudin, “Coastal resort life cycle: An  
370 overview of tioman island, malaysia,” *Tourism Planning & Development*, vol. 12, no. 3, pp.  
371 266–280, 2015.

- 372 [57] B. Hoeksema, Z. Waheed, and N. de Voogd, “Partial mortality in corals overgrown by the  
373 sponge *terpios hoshinota* at tioman island, peninsular malaysia (south china sea),” *Bulletin*  
374 *of marine science*, vol. 90, no. 4, pp. 989–990, 2014.
- 375 [58] R. Suriadi, H. Shaari, S. J. Culver, M. L. Husain, V. Vijayan, P. R. Parham, A. Sulaiman,  
376 and N. Sapon, “Inner shelf benthic foraminifera of the south china sea, east coast peninsular  
377 malaysia,” *Journal of Foraminiferal Research*, vol. 49, no. 1, pp. 11–28, 2019.
- 378 [59] S. Chowdhury and F. Mémoli, “Persistent path homology of directed networks,” in *Proceedings*  
379 *of the Twenty-Ninth Annual ACM-SIAM Symposium on Discrete Algorithms*. SIAM, 2018,  
380 pp. 1152–1169.
- 381 [60] D. Kozlov, “Discrete morse theory,” *Combinatorial algebraic topology*, pp. 179–209, 2008.
- 382 [61] H. J. Van Veen, N. Saul, D. Eargle, and S. W. Mangham, “Kepler mapper: A flexible python  
383 implementation of the mapper algorithm.” *Journal of Open Source Software*, vol. 4, no. 42, p.  
384 1315, 2019.